Population study for γ-ray pulsars with the outer gap model – II. Millisecond pulsars

J. Takata,* Y. Wang* and K. S. Cheng*

Department of Physics, University of Hong Kong, Pokfulam Road, Hong Kong

ABSTRACT

The population of γ-ray emitting millisecond pulsars (MSPs) was studied by using Monte Carlo techniques. We simulated the Galactic distributions of the MSPs, and applied the outer gap model for the γ-ray emission from each simulated MSP. We took into account the dependence of the observed γ-ray flux on the viewing angle and on the inclination angle, which is the angle between the rotation axis and the magnetic axis, respectively. Using the sensitivity of the 6-month long observation of the *Fermi* telescope and radio sensitivities of existing pulsar surveys, 9–13 radio-selected and 22–35 γ-ray-selected pulsars are detected within our simulation. The statistical properties of the simulated population are consistent with the *Fermi* observations. Scaling the observed sensitivity $\propto \sqrt{T}$, where T is the length of observation time, the present model predicts that over the 5-year mission *Fermi* would detect 15–22 radio-selected γ-ray MSPs, and 95–152 γ-ray-selected MSPs. Our simulation also predicts that about 100 (or 200–300) γ-ray MSPs with a flux larger than $F \geq 10^{-11}\,\mathrm{erg\,cm^{-2}\,s^{-1}}$ (or $5 \times 10^{-12}\,\mathrm{erg\,cm^{-2}\,s^{-1}}$) irradiate the Earth. With the present sensitivities of radio surveys, most of them are categorized as γ-ray-selected pulsars, indicating that most of the γ-ray MSPs have been missed by the present *Fermi* observations. We argue that the Galactic *Fermi* unidentified sources located at high latitudes should be dominated by MSPs, whereas the sources in the Galactic plane are dominated by radio-quiet canonical pulsars. We want to emphasize that the predicted number of radio-loud γ-ray MSPs depends on the sensitivities of radio surveys and that it can be increased, for example, from 15–22 to 26–37 if the radio sensitivity is improved by a factor of 2.

Key words: radiation mechanisms: non-thermal – methods: statistical – stars: neutron – pulsars: general – gamma-rays: stars.

1 INTRODUCTION

The millisecond pulsars (MSPs), which have a rotation period $P \sim 0.002$–$0.1\,\mathrm{s}$ and a stellar magnetic field $B_s \sim 10^{8-9}\,\mathrm{G}$, are classified as a different generation from the canonical pulsars, which have $P \sim 0.03$–$10\,\mathrm{s}$ and $B_s \sim 10^{12-13}\,\mathrm{G}$. The *Fermi* LAT has detected γ-ray emissions from about 60 pulsars in just 2 years of observation, including nine MSPs (Abdo et al. 2010a,b,c, 2009a,b; Saz Parkinson et al. 2010). Furthermore, the detection of radio MSPs from about 20 unidentified *Fermi* point sources (e.g. Caraveo 2010; Ray 2010; Ransom et al. 2011) has been reported. The MSPs are now recognized as one of the major populations of the Galactic γ-ray sources.

The particle acceleration and high-energy γ-ray radiation processes in the pulsar magnetosphere have been studied with the polar

cap model (Ruderman & Sutherland 1975; Daugherty & Harding 1982 ,1996), the slot gap model (Arons 1983; Muslimov & Harding 2003; Harding et al. 2008) and the outer gap model (Cheng, Ho & Ruderman 1986a,b; Hirotani 2008; Takata, Wang & Cheng 2010a), respectively. All models have assumed that the charged particles are accelerated by the electric field along the magnetic field lines, and that the accelerating electric field arises in the charge deficit region, where the local charge density deviates from the Goldreich–Julian charge density (Goldreich & Julian 1969). The polar cap model assumes that the acceleration region is near the stellar surface. On the other hand, the outer gap model and the slot gap model assume a strong acceleration region extending to the outer magnetosphere. For the canonical γ-ray pulsars, several access of observational evidence have been proposed for the outer magnetospheric origin of the γ-ray emissions (Aliu et al. 2008; Abdo et al. 2009c). Because the strength of the magnetic field at the outer magnetosphere of the MSPs is similar to that of canonical pulsars, $B \sim 10^{5-6}\,\mathrm{G}$, it is expected that if the γ-ray emissions of the MSPs originates from the

*E-mail: takata@hku.hk (JT); yuwang@hku.hk (YW); hrspksc@hkucc.hku.hk (KSC)

outer magnetosphere, the emission characteristics (e.g. pulse profile and spectrum) will be similar to those of the canonical pulsars.

Romani & Watters (2010) and Watters & Romani (2011) studied the pulse profiles of the canonical pulsars observed by *Fermi*. They computed the pulse profiles predicted by the outer gap model and slot gap model, and argued statistically that the outer gap geometry is more consistent with the observations than the slot gap geometry. Venter, Harding & Guillemot (2009) fit the pulse profiles of the *Fermi* detected MSPs with the geometries predicted by the different high-energy emission models. They found that the pulse profiles of two out of eight MSPs cannot be fitted by the geometry of either the outer gap model or the slot gap model. They proposed a pair-starved polar cap model, in which the multiplicity of the pairs is not high enough to completely screen the electric field above the polar cap, and the particles are continuously accelerated up to a high altitude over the entire open field line region. Thus we see that the γ-ray emission mechanism and the emission site in the MSP's magnetosphere have not been satisfactorily explained up to now.

The increase in population of detected γ-ray emitting pulsars allows us to perform a more detailed population study of the high-energy emissions from the pulsars. A comparison between the simulated and observed distributions of the various pulsar characteristics (e.g. rotation period and γ-ray flux) will be useful to test the high-energy emission model. With the canonical γ-ray pulsars, Takata, Wang & Cheng (2011) have studied the population predicted by the outer gap model. They predicted that with the sensitivity of the 6-month long *Fermi* observation, about 100 γ-ray emitting canonical pulsars can be detected, suggesting that the present observations have missed many γ-ray emitting pulsars. For the MSPs, Story, Gonthier & Harding (2007) have studied the population of γ-ray MSPs with the slot gap accelerator models and predicted the *Fermi* observations. They predicted that *Fermi* will detect 12 radio-loud and 33–40 radio-quiet γ-ray MSPs.

The Galactic population of the γ-ray pulsars has been studied for an understanding of the origin of the unidentified γ-ray point sources and diffuse background radiation (e.g. Bailes & Kniffen 1992; Faucher-Giguère & Loeb 2010). For example, Kaaret & Cottam (1995) argued that the EGRET unidentified sources near the Galactic plane are likely dominated by canonical pulsars. Faucher-Giguère & Loeb (2010) pointed out that the MSPs could provide a large contribution to the γ-ray background radiation at higher Galactic latitude. In the *Fermi* first source catalogue, there are several hundred unidentified steady point sources (Abdo et al. 2010b). Takata et al. (2011) have demonstrated that the *Fermi* unidentified sources located in the high Galactic latitudes cannot be explained by the Galactic distribution of the canonical pulsars. The MSPs are possible candidates for the high Galactic *Fermi* unidentified sources.

In this paper, we develop a Monte Carlo study of the population of the γ-ray emitting MSPs predicted by the outer gap model. In particular, we only study the population of MSPs in the Galactic field (not in the globular clusters). Following the previous studies (e.g. Cheng & Zhang 1998; Story et al. 2007; Takata et al. 2011), we will perform a Monte Carlo simulation for the Galactic population of the MSPs (Section 2). In Section 2.4, we will discuss our γ-ray emission model, including dependence of the γ-ray flux on the viewing geometry. In Section 3, we present the results of our simulation. In particular, we will compare the simulated population with the *Fermi* 6-month long observation (Section 3.2). In Section 3.4, we discuss the possibility of MSPs as the origin of the Galactic *Fermi* unidentified sources. We will discuss the results of our simulation in Section 4.

2　MONTE CARLO SIMULATION

2.1　Galactic population

In this study, we assume that all MSPs are born through the so-called recycled process in the low-mass binary systems, with a birth rate of $10^{-6} \sim 10^{-5}$ yr^{-1} (Lorimer et al. 1995; Lorimer 2008). The birth location is determined by the spatial distributions proposed by Paczynski (1990):

$$\rho_R(R) = \frac{a_R \mathrm{e}^{-R/R_{\exp}} R}{R_{\exp}^2},$$

$$\rho_z(z) = \frac{1}{z_{\exp}} \mathrm{e}^{-|z|/z_{\exp}}, \tag{1}$$

where R is the axial distance from the axis through the Galactic Centre perpendicular to the Galactic disc and z is the distance from the Galactic disc. In addition, $R_{\exp} = 4.5$ kpc, $a_R = [1 - \mathrm{e}^{-R_{\max}/R_{\exp}}(1 + R_{\max}/R_{\exp})]^{-1}$ with $R_{\max} = 20$ kpc and $z_{\exp} = 200$ pc (Story et al. 2007).

To obtain the current position of each simulated MSP, we solve the equations of motion from its birth to the current time. The equations of motion are given by

$$\frac{\mathrm{d}R^2}{\mathrm{d}t^2} = \frac{v_\phi^2}{R} - \frac{\partial \Phi_{\mathrm{tot}}}{\partial R}, \tag{2}$$

$$\frac{\mathrm{d}z^2}{\mathrm{d}t^2} = -\frac{\partial \Phi_{\mathrm{tot}}}{\partial z}, \tag{3}$$

and

$$R v_\phi = \mathrm{constant}. \tag{4}$$

Here v_ϕ is the azimuthal component of the velocity; $\Phi_{\mathrm{tot}} = \Phi_{\mathrm{sph}} + \Phi_{\mathrm{dis}} + \Phi_{\mathrm{h}}$ is the total gravitational potential, where Φ_{sph}, Φ_{dis} and Φ_{h} are the spheroidal, the disc and the halo components of the Galactic gravitational potential, and are given by

$$\Phi_i(R, z) = -\frac{G M_i}{\sqrt{R^2 + [a_i + (z^2 + b_i^2)^{1/2}]^2}}, \tag{5}$$

where $i = \mathrm{sph}$ and dis. For the spheroidal component, $a_{\mathrm{sph}} = 0$, $b_{\mathrm{sph}} = 0.277$ kpc and $M_{\mathrm{sph}} = 1.12 \times 10^{10}$ M$_\odot$. For the disc component, $a_{\mathrm{dis}} = 3.7$ kpc, $b_{\mathrm{dis}} = 0.20$ kpc, and $M_{\mathrm{dis}} = 8.07 \times 10^{10}$ M$_\odot$, while for the halo component

$$\Phi_{\mathrm{h}}(r) = -\frac{G M_{\mathrm{c}}}{r_{\mathrm{c}}} \left[\frac{1}{2} \ln \left(1 + \frac{r^2}{r_{\mathrm{c}}^2} \right) + \frac{r_{\mathrm{c}}}{r} \tan^{-1} \left(\frac{r}{r_{\mathrm{c}}} \right) \right], \tag{6}$$

where $r_{\mathrm{c}} = 6.0$ kpc and $M_{\mathrm{c}} = 5.0 \times 10^{10}$ M$_\odot$, respectively (cf. Burton & Gordon 1978; Binney & Tremaine 1987; Paczynski 1990). The Lagrangian in units of energy per unit mass is given by

$$L = \frac{v^2(R, z, \phi)}{2} - \Phi_{\mathrm{tot}}(R, z), \tag{7}$$

where v is the velocity of the pulsar.

For the distribution of the initial velocities of the MSPs, we assume a Maxwellian distribution with a characteristic width of $\sigma_v = 70$ km s^{-1} (cf. Hobbs et al. 2005), namely,

$$\rho_v(v) = \sqrt{\frac{\pi}{2}} \frac{v^2}{\sigma_v^3} \mathrm{e}^{-v^2/2\sigma_v^2}. \tag{8}$$

For the azimuthal component, the circular velocity due to the Galactic gravitational potential field at the birth position of the MSPs is taken into account, and it is calculated from

$$v_{\mathrm{circ}} = \left[R \left(\frac{\partial \Phi_{\mathrm{sph}}}{\partial R} + \frac{\partial \Phi_{\mathrm{dis}}}{\partial R} + \frac{\partial \Phi_{\mathrm{h}}}{\partial R} \right) \right]^{1/2}. \tag{9}$$

2.2 Pulsar characteristics

It is widely accepted that the MSPs are so-called recycled pulsars, which were spun up by accretion of the matter from the low-mass companion star. The rotation period of the newly born MSP is related to the history of the accretion on to the neutron star. In particular, its rotation period in the accretion stage may be related to the equilibrium spin period, $P_{eq} \sim 1.7 B_8^{6/7} \dot{M}_{15}^{-3/7} R_6^{18/7} M_{1.4}^{-5/7}$, where B_8 is the neutron star magnetic field in units of 10^8 G, $\dot{M}_{15}$ is the accretion rate in units of 10^{15} g s^{-1}, R_6 is the neutron star radius in units of 10^6 cm and $M_{1.4}$ is the neutron star mass in units of 1.4 solar mass (Frank, King & Raine 2002). However, the description of the transition from an accretion-powered to a rotation-powered phase is not well understood due to the complexities in the description of the interaction between the magnetosphere of a neutron star and its accretion disc. Furthermore, the transition, for which a rapidly decreasing accretion rate is required (e.g. Jeffrey 1986), may be facilitated by different processes between the long and short orbital period systems. For the long orbital period systems, a red giant companion can detach from its Roche lobe as its envelope is exhausted. On the other hand, for the short orbital period systems, a possible mechanism leading to the sudden decrease in the accretion flow is the operation of the so-called 'propeller effect' (Campana et al. 1998), or dissolution of the disc by γ-ray irradiation in the quiescent stage (Takata, Cheng & Taam 2010b). The initial period of the MSPs will depend on the characteristics of the orbital motion and/or the termination mechanism of the accretion flow.

In the present study, we assume that all MSPs are not directly produced by supernova explosions, but that they are born by the recycled process in a low-mass binary system. On this assumption, the true age of the MSPs, defined by the time since the neutron star was born in the supernova explosion, is different from the spin-down age (i.e. $P/2\dot{P}$), and from the age defined by activating the rotation-powered activity. Because the time-scale of the recycled process, including the decay of the neutron star's magnetic field and the accretion process, is not understood well, it is very difficult to calculate the present period and the magnetic field strength of MSPs from their initial distributions and the true age of MSPs.

Allowing for uncertainties, we use the observed distribution of the radio MSPs to assign 'current' pulsar characteristics (e.g. rotation period, magnetic field) for each simulated MSP, instead of modelling the initial distribution. In the usual Monte Carlo studies for the Galactic population of pulsars (e.g. Story et al. 2007; Takata et al. 2011), the initial period is assigned for each simulated pulsar and then the current position and rotation period are obtained. In the present study, on the other hand, we (1) generate the simulated MSPs with a constant birth rate over 10 Gyr, (2) obtain the current position as described in Section 2.1 and (3) assign the pulsar parameters following the observed distributions. Specifically, we assign the period time derivative ($\dot{P}$) and the stellar magnetic field (B_s) for each simulated MSP following the observed $\dot{P}$–B_s distribution, where we use the intrinsic value after removing the Shklovskii effect (see below). In this paper, we denote as B_s the strength of the magnetic field at the magnetic equator, namely, $B_s = 3.2 \times 10^{19} \sqrt{P\dot{P}}$. The current rotation period and the spin-down age of simulated MSPs are calculated from

$$P_{-3} = 0.97 B_8^2 \dot{P}_{-20}^{-1} \text{ ms} \tag{10}$$

and

$$\tau = 1.5 \times 10^9 P_{-3} \dot{P}_{20}^{-1} \text{ yr}, \tag{11}$$

respectively (Lyne & Graham-Smith 2006). Here P_{-3} and $\dot{P}_{-20}$ are the rotation period in units of 0.001 s and the period time derivative in units of 10^{-20}, respectively. The distributions, which are used in the present simulation, are represented for the various characteristics of the simulated MSPs in Fig. 1 by dashed lines. Fig. 1 also presents the observed distributions (shaded histograms; Manchester et al. 2005).

Shklovskii (1970) argued that the Doppler shift resulting from the transverse motion of a pulsar makes a positive contribution to the pulsar's period time derivative as (Manchester 1999)

$$\dot{P}_s = \frac{P\mu^2 d}{c}, \tag{12}$$

where μ is the proper motion of the MSP. For the MSPs whose period time derivative is extremely small, the Shklovskii effect may significantly increase the period time derivative. For canonical pulsars, on the other hand, the period time derivative is large, e.g. $\dot{P} \sim 10^{-13}$–10^{-15}, which is much greater than that caused by the Shklovskii effect.

We note that the present procedure can be applied if the Galactic distribution of the MSPs does not depend on the age of the rotation-powered MSPs (and spin-down age); that is, the Galactic MSP's populations of 1- and 10-Gyr MSPs, for example, are described by the same distribution. With the present assumption that all MSPs are born through the recycled process, which has a characteristic time-scale completely independent of the spin-down age, the Galactic distribution is independent of the distribution of the spin-down age. With a typical velocity of the observed MSPs, $v \sim 70$ km s^{-1}, it is expected that the typical displacement of MSPs with an age, $\tau \geq 100$ Myr, becomes larger than the size of the Galaxy. However, with the slow velocity, the MSPs remain bound to the Galaxy and hence their Galactic distribution does not depend on the age of the rotation-powered MSPs. On the other hand, for canonical pulsars (in particular for the γ-ray pulsars), the Galactic distribution depends on the true age, which is almost equal to the spin-down age. This allows us to calculate the present-period distribution from the initial distribution.

2.3 Radio emissions

Using the empirical relations among the radio luminosity, rotation period and period time derivative, the distribution of the radio luminosity at 400 MHz is expressed by (Narayan & Ostriker 1990)

$$\rho_{L_{400}} = 0.5\lambda^2 e^\lambda, \tag{13}$$

where $\lambda = 3.6[\log_{10}(L_{400}/\langle L_{400}\rangle) + 1.8]$ with $L_{400} = \eta 10^{6.64} \dot{P}^{1/3}/P^3$, and L_{400} is the luminosity in units of mJy kpc^2. Here η is a scaling factor to adjust the observed distribution, and $\eta = 1$ for the canonical pulsars. In the present simulation for the MSPs, we find that $\eta \sim 0.05$ can explain the distribution of the observed radio luminosity of the MSPs. The radio flux on Earth is given by $S_{400} = L_{400}/d^2$, where d is the distance to the MSP. We scale the simulated 400 MHz luminosity to the observational frequency using a typical photon index ~ 1.8 (Kramer et al. 1997).

We also take into account the beaming effect of the radio emissions. The half-angle, which is measured from the magnetic axis, of the radio emission cone of the MSPs does not depend on the frequency, and is approximately described by (Kramer & Xilouris 2000)
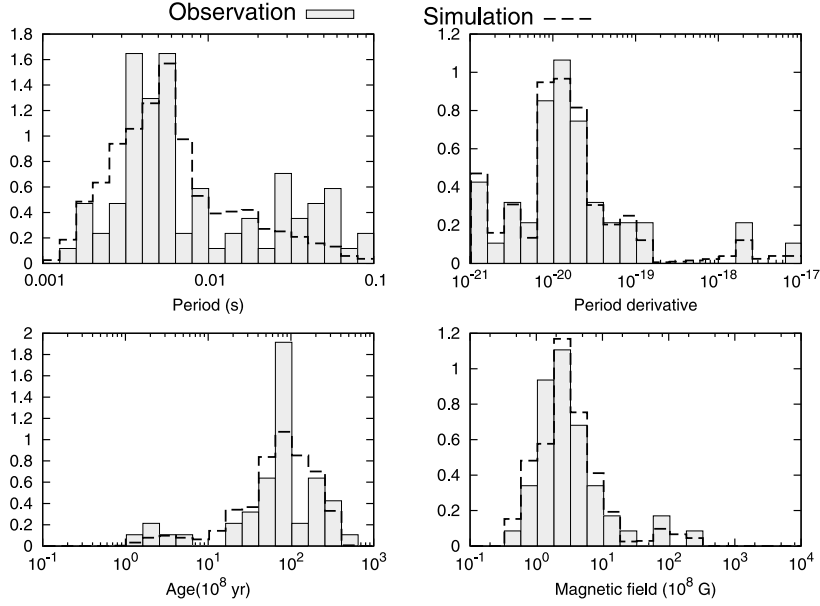
$$\omega \sim 5°.7 P^{-1/2}. \tag{14}$$

Figure 1. The observed distributions (shaded histograms) of the various characteristics for radio MSPs. The dashed lines show the distributions applied for the present simulation. The observed distributions are for the intrinsic values (i.e. without Shklovskii effect) of the pulsar parameters.

This emission can be detected by observers with a viewing angle between $\max(0°, \alpha - \omega)$ and $\min(\alpha + \omega, 90°)$, where α is the inclination angle between the rotation axis and the magnetic axis.

We use the 10 radio surveys (Molongo 2, Green Band 2 and 3, Arecibo 2 and 3, Parks 1, 2 and MB, Jordell Bank 2 and Swinburne IL), whose system characteristics are listed in table 1 of Takata et al. (2011) and the references therein. To calculate the dispersion measure, we use the Galactic distribution of electrons obtained by Cordes & Lazio (2002).

2.4 γ-ray emission model

2.4.1 Observed γ-ray flux

In this paper we apply the outer gap accelerator model (Cheng et al. 1986a,b; Zhang & Cheng 2003; Takata et al. 2010a) for the MSPs. In the outer gap, the electrons and/or positrons are accelerated up to a Lorentz factor of $\Gamma \geq 10^7$ by the electric field along the magnetic field line. These accelerated particles can emit γ-ray photons of several GeV through the curvature radiation process. Assuming a force balance between the electric force and the radiation drag force, the Lorentz factor is given by

$$\Gamma = \left(\frac{3R_c^2}{2e}E_{||}\right)^{1/4}, \qquad (15)$$

where R_c is the curvature radius of the magnetic field lines and $E_{||}$ is the accelerating electric field. The accelerating electric field in the outer gap is approximately given by (Cheng et al. 1986a,b; Cheng, Ruderman & Zhang 2000)

$$E_{||}(r, z) \sim \frac{B(r)f(r)^2 R_{lc}}{R_c}\frac{z}{z_h}\left(1 - \frac{z}{z_h}\right), \qquad (16)$$

where $R_{lc} = cP/2\pi$ is the light cylinder radius and $f(r)$ is the gap thickness divided by the light cylinder radius ($R_{lc} = cP/2\pi$) in the poloidal plane. In addition, z is the height measured from the last-open field line in the poloidal plane, and $z = z_h$ is the upper boundary of the gap. We note $B(r)f(r)^2 \sim$constant along the field line for the dipole field geometry.

The spectrum of the curvature radiation emitted by an individual particle may be written as

$$P_c(E_\gamma, r) = \frac{\sqrt{3}e^2\Gamma}{hR_c}F(x), \qquad (17)$$

where $x = E_\gamma/E_c$ with $E_c = 3hc\Gamma^3/4\pi R_c$ and

$$F(x) = x \int_x^\infty K_{5/3}(t)dt,$$

where $K_{5/3}$ is the modified Bessel function of order 5/3. If the γ-ray beam points towards an observer, the observer will measure a phase-averaged spectrum of (Hirotani 2008)

$$\frac{dF_\gamma}{dE_\gamma} \sim \frac{1}{d^2}\int N(r_\xi)R_c(r_\xi)P_c(E_\gamma, r_\xi)dA, \qquad (18)$$

where $N = B/Pce$ is the particle number density, r_ξ represents the radius from which the emission can be measured by the observer and dA is the cross-section of the gap perpendicular to the magnetic field lines. We assume that the outer gap extends in the azimuthal direction with $\delta\phi \sim \pi$ radian. The integrated energy flux between 100 MeV and 300 GeV can be calculated from

$$F_{\gamma, >100\,\mathrm{MeV}} = \int_{100\,\mathrm{MeV}}^{300\,\mathrm{GeV}}\frac{dF_\gamma}{dE_\gamma}dE_\gamma. \qquad (19)$$

One can show that the γ-ray flux described by equation (19) approximately satisfies $F_{\gamma, >100\,\mathrm{MeV}} \propto f(R_{lc})^3 L_{sd}$, where $L_{sd} = 4(2\pi)^4 B_s^2 R^6/6c^3 P^4$ is the spin-down power. If the typical energy of a curvature photon E_c satisfies $100\,\mathrm{MeV} \leq E_c \leq 100$ GeV, the power radiated by a single charged particle is $\int P_c dE_\gamma \sim 2e^2c\Gamma^4/3R_c^2$. Furthermore, if we estimate the total number of charged particles in the gap in terms of values near the light cylinder as $N_{gap} \sim \frac{B(R_{lc})}{Pce}R_{lc}\delta A(R_{lc})$, we obtain

$$F_{\gamma, >100\,\mathrm{MeV}} \sim \frac{1}{d^2}\frac{2e^2c\Gamma^4}{3R_{lc}^2}N_{gap} \sim \frac{f^3 B^2(R_{lc})R_{lc}^3\delta\phi}{d^2 P}$$

$$\propto \frac{f^3 B_s^2 R_s^6}{d^2 P^4 c^3} \propto f^3 L_{sd}/d^2, \qquad (20)$$

where we have used $\Gamma \sim (3R_{lc}^2 E_\parallel/2e)^{1/4}$, $E_\parallel \sim B(R_{lc})f^2(R_{lc})$ and $\delta A \sim f\delta\phi R_{lc}^2$. The γ-ray flux is proportional to the cube of the fractional gap thickness and the spin-down power.

We also assume as a zeroth-order approximation that the gap current is of the order of the Goldreich–Julian value over the full width. A detailed calculation of the outer gap model (e.g. Takata, Chang & Shibata 2008) gives the current distributions in the direction perpendicular to the magnetic field lines. On the other hand, by fitting the observed γ-ray spectra of all mature pulsars detected by *Fermi*, Wang, Takata & Cheng (2010) find that the total current in the gap is of the order of the Goldreich–Julian value. We expect that as long as the total power of the γ-ray radiation from the outer gap accelerator is concerned, the uniform current distribution with the Goldreich–Julian value would not be a bad approximation.

2.4.2 Thickness of the outer gap

Let us discuss now the thickness of the outer gap accelerator. Zhang & Cheng (2003) estimated the gap thickness for the MSPs when the photon–photon pair-creation process controls the gap activities. They have argued that the gap thickness is controlled by the photon–photon pair-creation process between the γ-rays emitted in the outer gap and the X-rays from the stellar surface, where the multiple magnetic field dominates the global dipole field (Ruderman 1991, Arons 1993). They estimated the typical gap thickness divided by the light cylinder radius at the light cylinder as

$$f_{ZC} = \frac{D_\perp(R_{lc})}{R_{lc}} = 7.0 \times 10^{-2} P_{-3}^{26/21} B_8^{-4/7} \delta r_5^{7/2}. \quad (21)$$

Here δr_5 is the distance (in units of 10^5 cm) from the stellar surface to the position where the local magnetic field is equal to the dipole field. In the following we assume that $\delta r_5 \sim 1$–10.

Takata et al. (2010a) proposed the outer gap model, in which the gap thickness is determined by the magnetic pair-creation process near the stellar surface. They argued that the returning particles, which were accelerated in the gap, will emit photons with an energy $m_e c^2/\alpha_f \sim 100$ MeV by curvature radiation near the stellar surface, where $m_e c^2$ and α_f are the electron rest mass energy and the fine structure constant, respectively. The 100 MeV photons form pairs by the magnetic pair creation process. The photon multiplicity is easily over 10^4 for each incoming particle. For a simple dipole field structure, all pairs should move inwards and cannot affect the outer gap accelerator. However, Takata et al. (2010a) have argued that if the magnetic field lines near the surface, instead of being nearly perpendicular to the surface, are bending sideways due to the strong local field, the pairs created on these local magnetic field lines can have an angle bigger than 90°, which would result in an outgoing flow of pairs. With this model, the estimated fractional gap thickness is given by

$$f_m = \frac{D_\perp(R_{lc})}{R_{lc}} \sim \frac{D_\perp(R_s)}{R_p} = 0.8\,K(P/1\,\mathrm{s})^{1/2}, \quad (22)$$

where $R_p \sim R_s(R_s/R_{lc})^{1/2}$ is the polar cap radius, $K \sim B_{m,12}^{-2} s_7$ is the parameter characterizing the local magnetic field properties, $B_{m,12}$ and s_7 are the local magnetic field in units of 10^{12} G and the local curvature radius in units of 10^7cm, respectively. By fitting the radiation properties of the γ-ray pulsars observed by *Fermi*, they find that $K \sim 2$ for the canonical pulsars, while $K \sim 15$ for the MSPs. When the fractional gap thickness f_m is smaller (or larger) than f_{zc}, the magnetic pair creation (or photon–photon pair creation) process controls the gap thickness.

Finally we discuss the maximum fractional thickness, f_{max}, for the active outer gap accelerator. Zhang & Cheng (1997) have argued that a pulsar with the fractional gap thickness larger than unity, $f_{zc} > 1$, is not active, because the pairs are not created in the gap by the photon–photon pair-creation process. However, the outer gap accelerator can exist only between the last-open field lines and the critical field lines, which are defined by those magnetic field lines that have the null point of the Goldreich–Julian charge density at the light cylinder. Therefore, we may define the maximum gap thickness as

$$f_{crit} = \frac{\theta_p - \theta_c}{\theta_p}, \quad (23)$$

where θ_p and θ_c are the polar angles of the last-closed field line and of the critical field line on the stellar surface, respectively. For the pure dipole field, we obtain

$$\theta_p = \alpha + \sin^{-1}\left[\sin(\theta_{lc} - \alpha)\left(\frac{R_s}{R_{lc}}\sin\theta_{lc}\right)^{1/2}\right] \quad (24)$$

and

$$\theta_c = \alpha + \sin^{-1}\left[\sin(\theta_n - \alpha)\left(\frac{R_s}{R_{lc}}\sin\theta_n\right)^{1/2}\right], \quad (25)$$

respectively, where

$$\theta_{lc} = \tan^{-1}\left(\frac{-3 - \sqrt{9 + 8\tan^2\alpha}}{4\tan\alpha}\right)$$

and

$$\theta_n = \tan^{-1}\left(\frac{3\tan\alpha + \sqrt{8 + 9\tan^2\alpha}}{2}\right).$$

In this paper, we examine two extreme cases corresponding to $f_{max} = 1$ and $f_{max} = f_{crit}$, respectively. The results for these two cases may give a range of uncertainty of the present theoretical predictions.

2.4.3 Dependence on the inclination and viewing angles

The observed characteristics of the γ-ray emissions depend on the viewing angle and the inclination angle between the rotation axis and the magnetic axis. With the geometry of the outer gap model, stronger emissions are emitted towards a viewing angle $\xi \sim 90°$, and the observed flux tends to decrease as the viewing angle closes to the rotation axis, where $\xi = 0°$ or $\xi = 180°$. To take into account this effect, we calculate the γ-ray flux, described in Section 2.4.1, as a function of the viewing angle and of the inclination angle. In the calculation, we apply the vacuum dipole field geometry and assume that the outer gap extends from the null charge point of the Goldreich–Julian charge density to $r = 1.5R_{lc}$ or $\rho = R_{lc}$, where ρ is the axial distance from the rotation axis. We also assume for simplicity no azimuthal dependence of the gap structure.

Fig. 2 shows the dependence of the γ-ray flux as a function of the viewing angle (ξ) and of the inclination angle (α). The vertical axis represents the fractional γ-ray flux, which is defined as the γ-ray flux divided by $f^3 L_{sd}/d^2$. The different lines correspond to the different inclination angles. The results are obtained for a rotation period $P = 3$ ms and the stellar magnetic field $B_s = 3 \times 10^8$ G. We can see in Fig. 2 that the calculated flux tends to decrease as both the viewing angle and the inclination angle decrease from 90°.
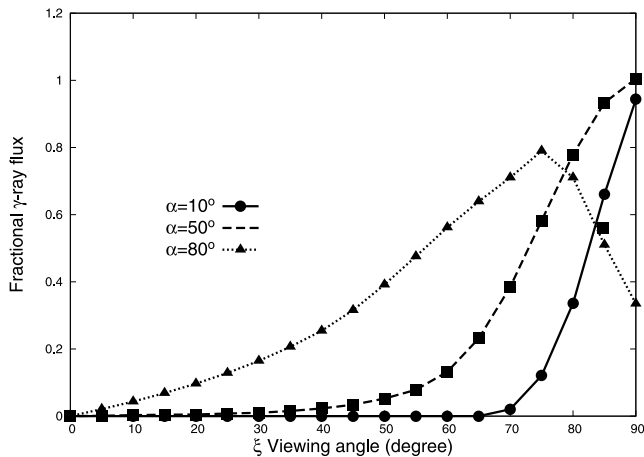
Figure 2. The fractional γ-ray flux as a function of the viewing angle and of the inclination angle. The fractional flux is defined by the ratio of the calculated flux measured on the Earth to $f^3 L_{sd}/d^2$. The results are for $P = 3$ ms, $B_s = 3 \times 10^8$ G and $f(R_{lc}) = 0.4$.

We can see that the general trend of the relation between the fractional γ-ray flux and the viewing angle and inclination angle, shown in Fig. 2, is maintained for different sets of the rotation periods and magnetic fields. In this study, for simplicity, we use the relations in Fig. 2 for all sets of the rotation period and magnetic field. We assume that the inclination angle and viewing angle are randomly distributed.

However, we do not take into account the dependence of the spin-down power on the inclination angle. The pulsar spin-down can result from both the current braking torque and the magnetic dipole radiation. The former can spin-down the pulsar even if the inclination angle is zero. According to the analysis of the force-free magnetosphere done by Spitkovsky (2006), the spin-down power depends on the inclination angles as $L_{sd} \propto 1 + \sin^2 \alpha$; in other words, L_{sd} changes only by a factor of 2 with the inclination angle. With this small variation, we may expect that the general properties

of the simulated distributions for the MSP's characteristics (such as the period and the magnetic field) are not affected much by dependence on the inclination angle.

3 RESULTS AND DISCUSSION

In the Monte Carlo simulations, we generated 3×10^6 MSPs with a constant birth rate over 10 Gyr. About 2100 radio MSPs were detected by the simulated radio surveys. Scaling the simulated population to the number of radio MSPs in the ATNF catalogue, ~ 80, we obtain $\sim 10^{-5}$ yr^{-1} as the predicted average birth rate, which is consistent, within the uncertainties, with the other population studies (e.g. Ferrario & Wickramasinghe 2007).

3.1 Galactic distribution of MSPs

In this section, we discuss the consistency of the observed and simulated distributions of the radio MSPs. First, Figs 3(a) and (b) compare the observed (shaded histograms) and simulated (dashed lines) distributions of the radio luminosity at 400 MHz and of distance, respectively. We can see that the simulated distribution (dashed lines) qualitatively explains the observed features; for example, the peak positions of the distributions. On the other hand, we find that it is difficult to explain the sharp peak at 1–2 kpc in the observed distribution of the distance. We argue that this excess in the observed distribution is caused by several MSPs, and that the excess may be produced by enhancements of the local medium (e.g. the Gould Belt) and of the local birth rate. For example, the age of the Gould Belt is believed to be $\sim 10^{7-8}$ yr (Grenier 2004). Because the birth rate of the canonical pulsars in the Gould Belt is expected to be one per 10^5 yr, and because the birth rates of the MSPs in the Galactic field are 2–3 orders smaller than that of the canonical pulsars, one may expect 1 per 10^{7-8} yr as the birth rate of the MSPs in the Gould Belt. This indicates that several MSPs can be born within the age of the Gould Belt. If one assumes that the typical radial velocity of MSPs is $(70/\sqrt{3}) \sim 40$ km s^{-1}, then the displacement from the
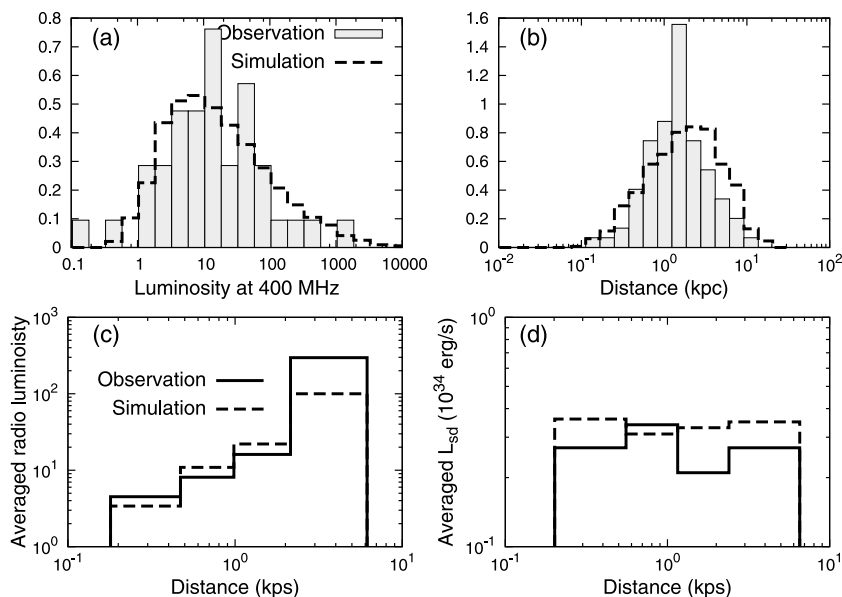

Figure 3. Distributions of (a) luminosity and (b) distance of the observed (shaded histograms) and simulated (dashed lines) radio MSPs. The panels (c) and (d) represent the average radio luminosity and the spin-down power for the observed (solid lines) and the simulated (dashed lines) MSPs as a function of the distance, respectively. Each bin of the solid lines contains the same number of the observed MSPs.

Gould Belt is $d \sim 5 \times 10^7\,\mathrm{yr} \times 40\,\mathrm{km\,s^{-1}} \sim 2\,\mathrm{kpc}$, which is consistent with the enhancement of the peak in the distribution of the distance.

Figs 3(c) and (d) show the average luminosity and spin-down power, respectively, as a function of the distance. The solid and dashed lines are the results from observations and simulations, respectively, and each bin of the histograms has the same number of observed MSPs. We find in Figs 3(c) and (d) that the present simulation describes characteristics of the observations very well, that is, the average radio luminosity increases with the distance and the average spin-down power is almost constant with the distance. Finally, we can see that the simulated MSPs can reproduce the Galactic longitude and latitude distributions of the radio MSPs. On these grounds, we conclude that our simulation reproduces the Galactic distribution of the radio MSPs.

3.2 Comparison with *Fermi* observations

In this section, we compare the results of our simulation with the *Fermi* 6-month long observations. *Fermi* has found nine 'radio-selected' γ-ray emitting MSPs with a flux $F_\gamma \geq 10^{-11}\,\mathrm{erg\,cm^{-2}\,s^{-1}}$ (Abdo et al 2009b; Abdo et al. 2010a,c), and that all of them are located at high Galactic latitudes, that is, $|b| \geq 5°$. Abdo et al. (2010a) show that the sensitivity of the low Galactic latitudes is about a factor of 3 worse as compared to that of high Galactic latitudes. In the present simulation, therefore, we use $F = 10^{-11}\,\mathrm{erg\,cm^{-2}\,s^{-1}}$ for the Galactic latitudes $|b| \geq 5°$ and $3 \times 10^{-11}\,\mathrm{erg\,cm^{-2}\,s^{-1}}$ for $|b| \leq 5°$ as the sensitivity requirement of the radio-selected MSPs for the 6-month long observations. Because no γ-ray-selected MSPs have been detected so far, we cannot simulate the *Fermi* sensitivity of the blind search for the MSPs. In this section, we show the results of our simulations by setting the sensitivity to that of the canonical pulsars, that is $F = 2 \times 10^{-11}\,\mathrm{erg\,cm^{-2}\,s^{-1}}$ for Galactic latitudes $|b| \geq 5°$ and $6 \times 10^{-11}\,\mathrm{erg\,cm^{-2}\,s^{-1}}$ for $|b| \leq 5°$.

Table 1 summarizes the population of the radio-selected and the γ-ray-selected MSPs detected within the simulations. N_r and N_g represent the population of the radio-selected and γ-ray-selected MSPs, respectively, detected with the *Fermi* 6-month sensitivity and $N_{i,F>10^{-10}}$ ($i =$ r, g) are the populations of 'bright' MSPs with a γ-ray flux larger than $10^{-10}\,\mathrm{erg\,cm^{-2}\,s^{-1}}$. In addition, $N_{i,5}$ and $N_{i,10}$ are the populations with sensitivity projected to 5- and 10-yr observations, respectively, for which the sensitivity is scaled $\propto \sqrt{T}$, where T is the length of the observation time.

As Table 1 shows, our model predicts that only 2–3 radio-selected and 1–3 γ-ray-selected MSPs can be detected with a flux larger $10^{-10}\,\mathrm{erg\,cm^{-2}\,s^{-1}}$. Although the results of the *Fermi* with the 6-month long observations (Abdo et al. 2009a) did not include the bright sources, it is possible that with the small population of the

Table 1. Population of the simulated radio-selected and γ-ray-selected γ-ray MSPs. The subscript r and g represent the radio-selected and γ-ray-selected pulsars, respectively. $N_{i,F>10^{-10}}$ ($i =$ r, g) are population of 'bright' MSPs with a γ-ray flux larger than $10^{-10}\,\mathrm{erg\,cm^{-2}\,s^{-1}}$, and N_i are results with the *Fermi* 6-month long observation. In addition, $N_{i,5}$ and $N_{i,10}$ are population with the sensitivity projected to 5- and 10-yr observations, respectively.

	$N_{r,F\geq 10^{-10}}$	$N_{g,F\geq 10^{-10}}$	N_r	N_g	$N_{r,5}$	$N_{g,5}$	$N_{r,10}$	$N_{g,10}$
$f_{max} = f_{crit}$	2	2	9	22	15	101	17	157
$f_{max} = 1$	3	3	13	35	22	161	25	248

bright MSPs, *Fermi* may have missed the detection of the pulsation. The *Fermi* unidentified catalogue includes about 50 sources with a flux larger than $10^{-10}\,\mathrm{erg\,cm^{-2}\,s^{-1}}$. We can see that the spectral behaviors of most of them are consistent with those of the known γ-ray pulsars: (1) they are steady sources in the sense that the variability index defined in Abdo et al. (2010b) is smaller than 23, and (2) the spectra above 100 MeV cannot be fitted well by single power law, that is, the curvature index, C (defined in Abdo et al. 2010b), is ≥ 10. Although most of them may be canonical γ-ray pulsars (cf. Takata et al. 2011) or active galactic nuclei (Abdo et al. 2010d), it is very likely that a small fraction, in particular, high Galactic sources, are γ-ray emitting MSPs (see Section 3.4). Recently, Ransom et al. (2011) reported the discovery of three radio MSPs associated with the *Fermi* unidentified bright sources, suggesting that our results are quite consistent with the observations.

Applying the sensitivity of *Fermi* 6-month long observation, our model predicts 9–13 radio-selected γ-ray MSPs, which is consistent with the nine MSPs with *Fermi* observations. We also predict 22–35 γ-ray-selected MSPs, whereas *Fermi* has had no such detections so far. For the canonical pulsars, the sensitivity of the blind search is about a factor of 2 worse as compared to that of the radio-selected pulsars (Abdo et al. 2010a). The population of the γ-ray-selected pulsars is roughly comparable with that of the radio-selected γ-ray pulsars. On the other hand, it is expected that the detection of the rotation period from the MSPs (in particular in binary systems) by the blind search is even harder and the sensitivity is much worse than that of the canonical pulsars.

Fig. 4 compares the cumulative distributions of the various characteristics of the observed nine (solid lines) γ-ray MSPs detected by *Fermi* (Abdo etal. 2009b; Abdo et al. 2010a,b,c) and the simulated (dashed lines) radio-selected γ-ray MSPs. The results are for $f_{max} = f_{crit}$. We performed a Kolmogorov–Smirnov (KS) test to compare the two cumulative distributions. In Fig. 4, we present the maximum deviation (D_{max}) between the two distributions and the p-value (P_{KS}) of the KS test for each pulsar characteristics. Since the simulated sample has more than 400 pulsars, we used the one-sample KS statistic. For example, the p-value for the rotation period is $P_{KS} \sim 0.75$, suggesting that the hypothesis that the two distributions are drawn from the same distribution cannot be rejected at better than 25 per cent confidence level. We find in Fig. 4 that for all distributions except that for the flux distribution, the hypothesis cannot be rejected at better than 60 per cent, indicating that the model distributions are consistent with the observations.

For the γ-ray flux (right-bottom panel in Fig. 4), the result of the KS statistic provides a relatively low p-value, as compared to other characteristics. This is because all the nine MSPs detected by *Fermi* have a γ-ray flux smaller than $10^{-10}\,\mathrm{erg\,cm^{-2}\,s^{-1}}$, while the model predicts that about 20 per cent of γ-ray MSPs have a flux larger than $10^{-10}\,\mathrm{erg\,cm^{-2}\,s^{-1}}$. However, we note that the difference between the observed and simulated distributions is caused by only one or two MSPs. Hence, if several MSPs with a bright γ-ray emissions of $F_\gamma \geq 10^{-10}\,\mathrm{erg\,cm^{-2}\,s^{-1}}$ have been missed by the *Fermi* observations, the model distribution is not in conflict with the observations. It is important to note that our simulation results are based on the existing radio sensitivities of pulsar surveys. Any deep radio search implies increasing the radio sensitivities and consequently some γ-ray-selected MSPs can become radio-loud. In fact, several radio MSPs have been detected by deep search for the radio emissions from bright *Fermi* unidentified sources (Ransom et al. 2011). These radio-loud γ-ray MSPs are defined as γ-ray-selected MSPs in our simulations.
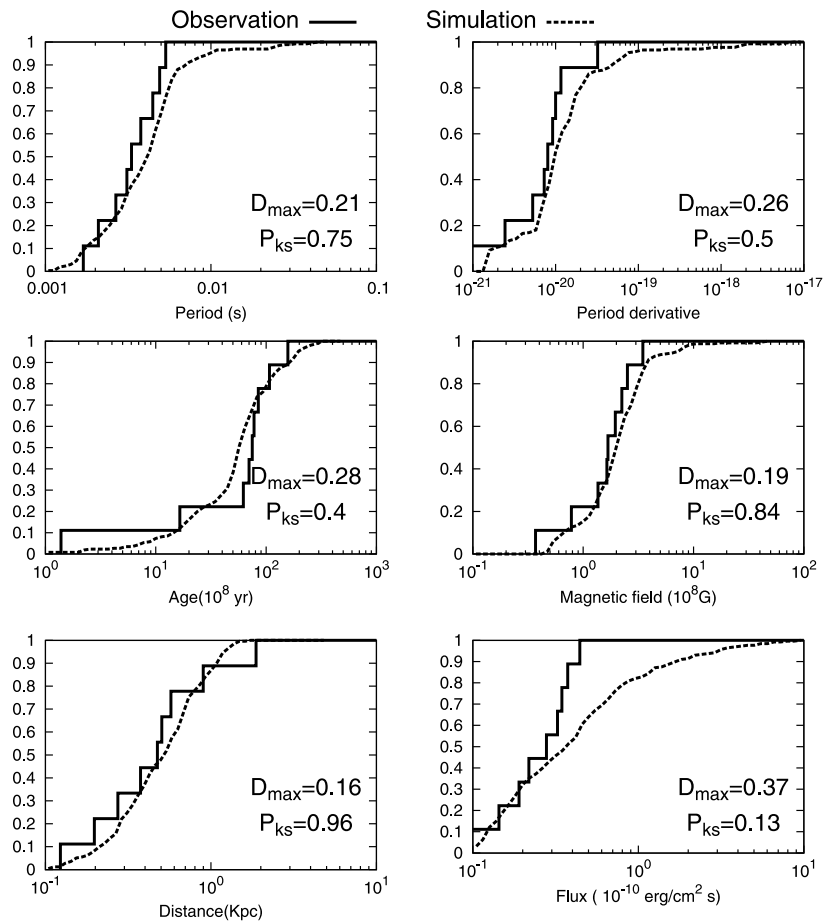
Figure 4. Cumulative distributions for the various characteristics of the observed (solid lines) and simulated (dashed lined) radio-selected γ-ray MSPs with the sensitivity of the *Fermi* 6-month long observation. The maximum difference (D_{max}) and the p-value of KS test (P_{KS}) are also displayed. The intrinsic values, that is, the values without the Shklovskii effect, are also represented.

Table 2. Population of the simulated radio-selected and γ-ray-selected MSPs for the different radio surveys and projected mission lengths of *Fermi* (6 months, 5 yr and 10 yr). A2 and P2 represent the Arecibo 2 and Parks 2 surveys. 'All' represents all radio surveys listed in table 1 of Takata et al. (2010b) and 'All× 2' shows the results from all the radio surveys but we increase the sensitivity of each survey by a factor of 2. In addition, the intrinsic populations, that is, the populations associated with only beaming effects of the radio emission, are shown in the bottom line. In this extreme limit, most *Fermi* γ-ray pulsars become radio-selected γ-ray pulsars.

	6 month				5 yr				10 yr			
	$f_{max} = f_{crit}$		$f_{max} = 1$		$f_{max} = f_{crit}$		$f_{max} = 1$		$f_{max} = f_{crit}$		$f_{max} = 1$	
	N_r	N_g	N_r	N_g	$N_{r,5}$	$N_{g,5}$	$N_{r,5}$	$N_{g,5}$	$N_{r,10}$	$N_{g,10}$	$N_{r,10}$	$N_{g,10}$
A2, P2	5	25	7	40	9	105	12	168	10	162	14	255
All	9	22	13	35	15	101	22	161	17	157	25	248
All (×2)	16	18	23	30	26	93	37	150	29	148	42	234
Intrinsic	61	3	88	6	226	10	329	27	331	16	484	41

As Table 1 shows, the model predicts that the population of radio-selected γ-ray MSPs increases by only about 10 over the 5 yr (or 10 yr) of *Fermi* observations. This implies that most of the presently known radio MSPs (∼80) might not be discovered by *Fermi*. However, the predicted radio-loud γ-ray MSPs depend on the sensitivity of radio surveys, as we can see in Table 2. For the γ-ray-selected MSPs, the simulation predicts that *Fermi* can detect at least 100 sources. As we will discuss in Section 3.4, we expect that these simulated γ-ray-selected MSPs correspond to the *Fermi* unidentified sources. As we have emphasized before, we predict that more and more radio MSPs will be confirmed

among the *Fermi* unidentified sources by a deep search of the radio emissions.

Story et al. (2007) studied the population of γ-ray MSPs by using the slot gap accelerator model and predicted that *Fermi* would detect about 12 radio-loud and 33–40 radio-quiet γ-ray MSPs. On the other hand, our outer gap model tends to predict more γ-ray (in particular radio-quiet) MSPs than the slot gap model. Also, the present simulation predicts a larger ratio between the radio-quiet and radio-loud MSPs (∼6–7) than that predicted by the slot gap model (∼3), although the ratio depends on the simulated sensitivities of the *Fermi* and radio observations (Sections 3.3 and 3.4).
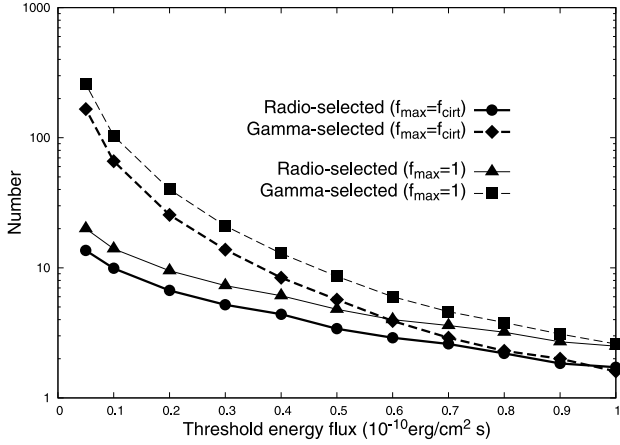
Figure 5. The simulated numbers of the radio-selected (solid line) and γ-ray-selected (dashed line) γ-ray MSPs as a function of the threshold energy flux.

3.3 Population of γ-ray MSPs

In Fig. 5, we summarize the population of the γ-ray emitting MSPs detected within the simulation as a function of the threshold energy flux of the γ-rays. The solid lines and dashed lines represent the population of the radio-selected and γ-ray-selected γ-ray MSPs, respectively. The thick and thin lines represent results for the maximum fractional gap thickness of $f_{max} = f_{crit}$ and $f_{max} = 1$, respectively. For example, the present simulation predicts that ∼2–3 and ∼10–14 radio-selected γ-ray MSPs irradiate the Earth with a γ-ray flux $F_\gamma \geq 10^{-10}$ and $F_\gamma \geq 10^{-11}$ erg cm^{-2} s^{-1}, respectively. For the radio-quiet γ-ray MSPs, about 100 sources with a flux larger than 10^{-11} erg cm^{-2} s^{-1} irradiate the Earth.

We can see in Fig. 5 that the number of γ-ray-selected MSPs increases more rapidly than that of the radio-selected γ-ray MSPs and that the ratio of the γ-ray-selected to radio-selected γ-ray MSPs increases with decreasing threshold energy flux. As the threshold of γ-ray energy flux decreases, the γ-ray emissions from more distant MSPs can be detected in the simulations. On the other hand, because we fix the sensitivity of the radio surveys in Fig. 5, the radio emissions from those distant MSPs may not be detected by the radio surveys. As a result, more γ-ray-selected MSPs are detected in the simulations as the threshold flux decreases. In fact, if we count all the γ-ray MSPs irradiating the Earth with radio emissions as the radio-selected pulsars, the ratio would not depend on the threshold energy flux of the γ-ray emissions.
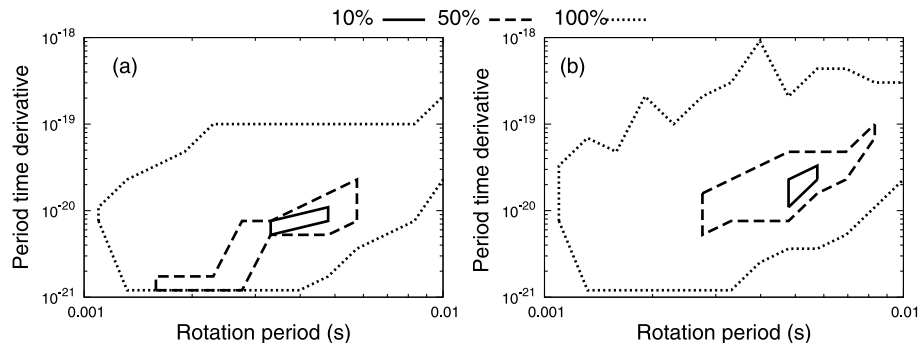
Fig. 6 shows contours of the two-dimensional distribution in the rotation period and the period-time derivative of the simulated MSPs with a γ-ray flux $F_\gamma \geq 10^{-11}$ erg cm^{-2} s^{-1}. We present the distributions of all the simulated MSPs including the radio-selected and γ-ray-selected pulsars, because the two distributions do not differ much from each other. The left-hand panel shows the distributions using the period time derivative for the intrinsic value, and the right-hand panel represents the period time derivative for the 'observed' value, that is, the value after adding the Shklovskii effect described by equation (12). The solid, dashed and dotted lines represent 10, 50 and 100 per cent of the total MSP population. We can see that the Shklovskii effect slightly shifts the peak of the distributions towards longer rotation periods and larger period time derivatives. For the observational distributions (right-hand panel), about 50 per cent of the γ-ray emitting MSPs can be detected with a rotation period of $P \sim 0.003$–0.008 s and a period time derivative $\dot{P} \sim 6 \times 10^{-21}$–$10^{-19}$. This information can be used to narrow down the parameter range for a blind search to detect the rotation period from *Fermi* unidentified sources.

3.4 Origin of the Galactic *Fermi* unidentified steady sources

As Fig. 5 shows, our simulation predicts that about ∼200 γ-ray MSPs irradiate the Earth with a flux $F_\gamma \geq 5 \times 10^{-12}$ erg cm^{-2} s^{-1} and with the present sensitivity of radio surveys most of them are categorized as γ-ray-selected MSPs. Therefore, it is likely that although millisecond pulsed emission has not been confirmed yet, the γ-ray MSPs contribute to the Galactic unidentified *Fermi* sources, such as the newly discovered 20 radio MSPs associated with the *Fermi* unidentified sources (Caraveo 2010; Ray 2010; Ransom et al. 2011).

Fig. 7 plots the curvature index (*C*) and the variability index (*V*) of the *Fermi* sources; a curvature index larger than 11.34 indicates a less than 1 per cent chance that the power-law spectrum is a good fit above 100 MeV, and a variability index larger than 23.21 indicates less than a 1 per cent chance of being a steady source [see Abdo et al. (2010b) for the exact definition of *C* and *V* indexes]. The filled circles, boxes and triangles correspond to the pulsars, active galactic nuclei (AGN) and *Fermi* unidentified sources. In Fig. 7, we can easily see that the pulsars and the AGN belong to different groups in the *C*–*V* plane, that is, the pulsars belong to $C \geq 5$ and $V \leq 20$, whereas AGN belong to wide range of variability index, which may indicate a correlation between the *C* index and *V* index (that is, $C \propto V$). Most of the *Fermi* unidentified sources have the *V* index smaller than ∼30, with the *C*-index larger than 0.1. Fig. 7

Figure 6. Contours of the two-dimensional (rotation period and period time derivative) distributions of the simulated MSPs with the sensitivity of the *Fermi* 6-month long observation; (a) intrinsic period time derivative and (b) 'observed' period time derivative adding Shklovskii effect. More MSPs are located within the solid lines. Within solid, dashed and dotted lines, 10, 50 and 100 per cent of the total MSPs are populated.
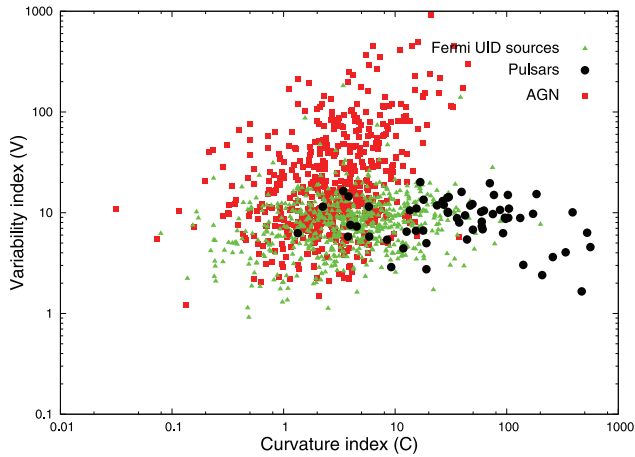
Figure 7. Plots for the curvature index and the variability index of the *Fermi* sources (Abdo et al. 2010b). The filled circles, and boxes and triangles are the pulsars, AGNs, and the *Fermi* unidentified sources, respectively.

indicates that the *Fermi* unidentified sources can be either pulsars or AGN.

In Fig. 8, we plot the Galactic distributions of the *Fermi* unidentified steady sources for $C < 5$ (solid line) and $C \geq 5$ (dashed line). It is clear from Fig. 8 that the two lines represent different distributions with respect to each other. The solid lines show relatively constant distributions for the Galactic longitudes and latitudes, indicating that most of the *Fermi* unidentified sources with $C < 5$ (dashed lines) distribute isotropically in the sky, and may be related to extragalactic (or Galactic halo) sources. For the dashed lines, on the other hand, the distributions for the Galactic longitudes and

latitudes coordinate show peaks at the Galactic Centre and at the Galactic disc, respectively, suggesting that the *Fermi* unidentified steady sources with $C \geq 5$ are associated with Galactic objects.

In Fig. 9, we compare the distributions of the Galactic longitudes (left-hand panel) and latitudes (right-hand panel) for the unidentified *Fermi* sources with $V \leq 23.21$ and $C \geq 5$ (solid line) and the simulated γ-ray MSPs (dashed line), with a flux $F_\gamma \geq 10^{-11}$ erg cm^{-2} s^{-1}. The latitude distribution of the γ-ray emitting canonical pulsars (dotted line) simulated in Takata et al. (2011) and the Galactic distributions for known radio MSPs (dotted lines) are also plotted in the figure.

In Figs 9 we can see that the distributions of the simulated γ-ray MSPs and of the observed radio MSPs are consistent with that of the *Fermi* unidentified sources, that is, (1) three longitude distributions have a peak around the direction of the Galactic Centre $l = 0°$ and become minimum around $l \sim 180°$, and (2) the latitude distributions have a peak at the Galactic plane ($b = 0$) and then they decrease with the increase of the Galactic latitudes. In particular, the MSPs can explain the distributions of the *Fermi* unidentified sources located above the Galactic plane $|b| \geq 10$, which cannot be explained by the canonical γ-ray pulsars, as the right-hand panel in Fig. 9 shows; the γ-ray emitting canonical pulsars can mainly explain the unidentified sources located in the Galactic plane. Since the MSPs are in general older than the canonical pulsars, a higher fraction of the γ-ray MSPs, as compared to the canonical pulsars, is located at higher Galactic latitudes. On these grounds, we conclude that γ-ray emitting MSPs are more plausible as candidates for the origin of the majority of the Galactic *Fermi* unidentified steady sources located in high Galactic latitudes.

We note that new radio MSPs have been discovered in the direction of about 20 unidentified *Fermi* sources by the radio searches
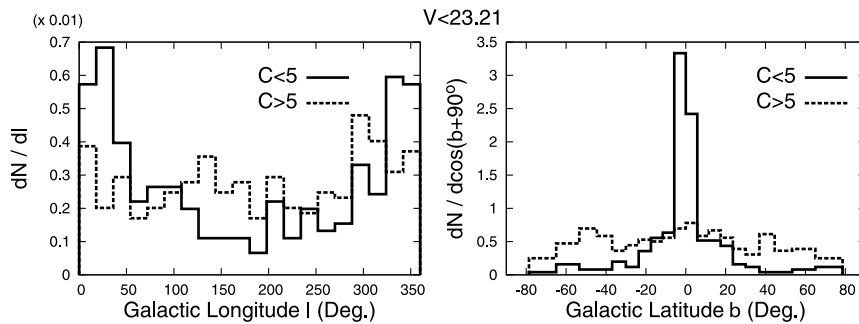

Figure 8. The distributions in Galactic coordinate longitudes (left) and latitudes (right) of the *Fermi* unidentified steady sources. The solid and dashed lines are the results for $C < 5$ and $C \geq 5$, respectively.
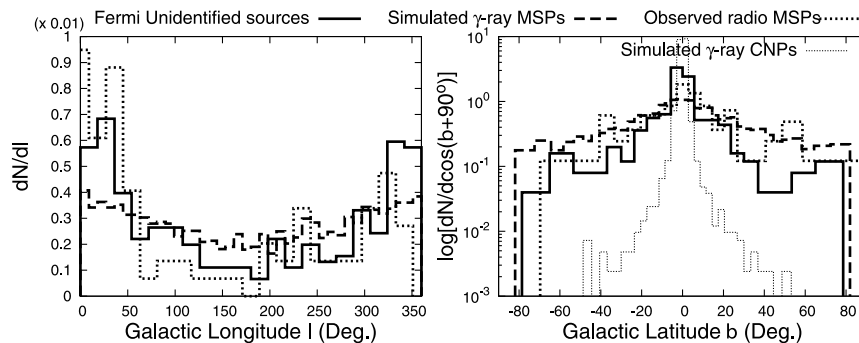

Figure 9. The distributions of Galactic longitudes (left) and latitudes (right) of the *Fermi* unidentified point sources with $V \leq 23.21$ and $C \geq 5$ (solid lines), the simulated γ-ray MSPs (dashed lines) and observed radio MSPs (dotted lines). The distribution of Galactic latitudes of the simulated γ-ray emitting canonical pulsars (CNP) in Takata et al. (2010b) are also plotted in the right-hand panel (thin dotted line).
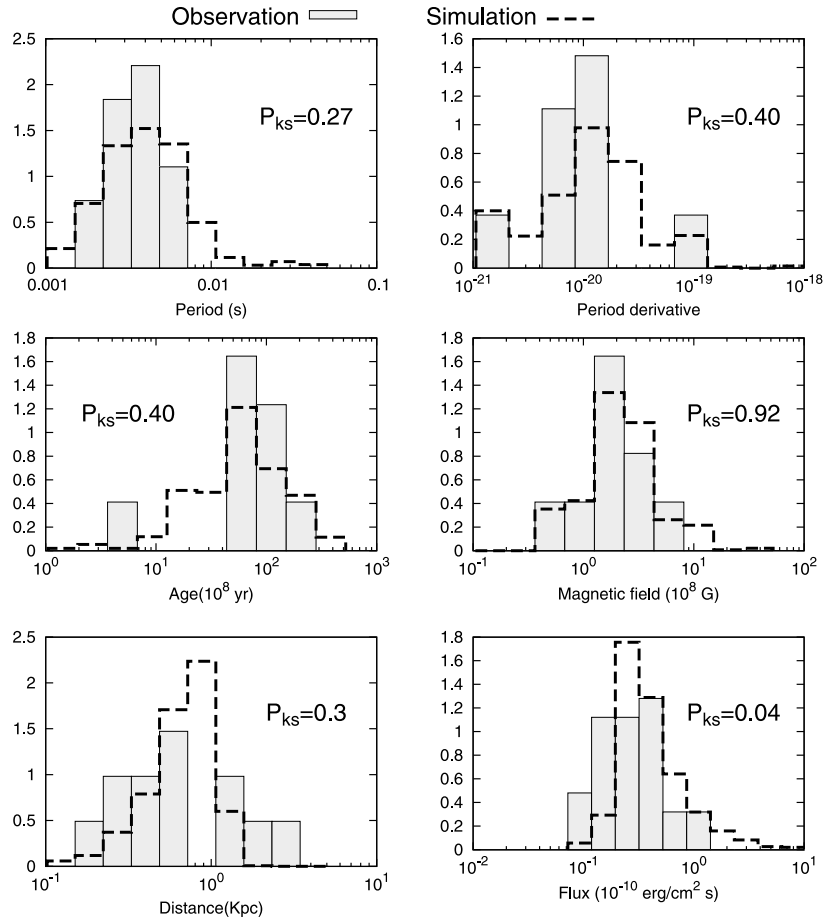
Figure 10. Distributions of the various properties of the observed (shaded histograms) and of the simulated (dashed lines) MSPs. In addition to the nine known γ-ray MSPs, the observed distributions of the rotation period and of the distance includes seven and three radio MSPs, respectively, associated with the *Fermi* unidentified sources. For the γ-ray flux, the observed distributions include 20 radio MSPs associated with the *Fermi* unidentified sources. For the simulation, both radio-selected and γ-ray-selected MSPs are included in the distributions.

for individual sources (e.g. Caraveo 2010; Ray 2010; Ransom et al. 2011). These *γ-ray-selected radio-loud* MSPs can be classified as the γ-ray-selected radio-quiet sources in the present simulation, because we do not take into account the radio search for the specific sources. In Table 2, on the other hand, we present how the population of γ-ray emitting MSPs depends on the sensitivity of radio surveys. We used the Arecibo 2 (A2) and Parks 2 (P2) surveys (the first row), all the radio surveys (the second row) listed in table 1 of Takata et al. (2011) and all radio surveys but we increase by a factor of 2 the sensitivity of each survey (third row). The intrinsic populations, that is, the populations associated with only beaming effects of the radio emission, are shown in the bottom row.

We can see in Table 2 that the number of radio-selected pulsars increases with increasing sensitivity of the radio surveys, whereas the number of γ-ray-selected pulsars decreases. This is because if we increase the sensitivity of the radio surveys, some of the γ-ray-selected MSPs irradiating the Earth with the radio emissions may be reclassified as radio-selected γ-ray pulsars. As the bottom row in Table 2 shows, the intrinsic ratio of the radio-loud and radio-quiet γ-ray MSPs is 10 ~ 20, indicating that most of the γ-ray emitting MSPs irradiate the Earth with a corresponding radio emission. Therefore, our prediction is that as the sensitivity of the radio observations will improve in the future, more and more radio MSPs will be discovered among the *Fermi* unidentified sources.

In Fig. 10, we present the distributions of the various characteristics of the observed γ-ray MSPs (shaded histograms), including the 20 new radio MSPs associated with *Fermi* unidentified sources, and the simulated γ-ray MSPs (dashed lines) with the simulated sensitivity of the *Fermi* 6-month long observation. For the simulated distribution, both the radio-selected and γ-ray-selected MSPs are taken into account. For the observations, we were able to obtain information of the rotation period for seven out of the 20 radio MSPs and the distances for three MSPs (Ray 2010; Ransom et al. 2011). Therefore, the distributions of the rotation period and of the distance in Fig. 10 are obtained from 16 (nine known *Fermi* MSPs plus seven radio MSPs) and 12 samples, respectively. The distributions of the period time derivative, the magnetic field and the spin-down age include only nine known *Fermi* MSPs, because we could not find any references for the intrinsic period time derivative of the 20 radio MSPs. The γ-ray fluxes of the 20 radio MSPs are taken from the *Fermi* first catalogue (Abdo et al. 2010b[1]) and Ransom et al. (2011). In Fig. 10, we also indicate the *p*-values (P_{ks}) of the KS test. As Fig. 10 shows, the simulated distributions are qualitatively consistent with the observations (e.g. the position of the peak of the distributions). For the γ-ray flux, however, the *p*-value of the KS test

---

[1] See also http://fermi.gsfc.nasa.gov/ssc/data/access/lat/1yr_catalog

is much lower than those of the other characteristics, indicating that the two distributions cannot be drawn from the same distribution. Because it is expected that the γ-ray emissions from the 20 radio MSPs associated with *Fermi* unidentified sources will be composed of a pulsed and an unpulsed component, the extraction of the pulsed component, that is, the detection of the pulsed period with *Fermi*, is required to constrain our model.

We have assumed that MSPs are activated as the rotation-powered pulsar as a result of the accretion process from the companion star. Recently Takata et al. (2010b) argued that the outer gap activities of MSPs can be turned on in the quiescent state of low-mass binary systems, for example PSR J1023+0038 (Archibald et al. 2009). The geometry of the outer gap can direct the γ-rays emitted from the gap towards the companion star and the accretion disc. Consequently, the accretion disc can be evaporated, and the companion star becomes brighter due to the irradiation of γ-rays. If the high-latitude unidentified sources of *Fermi* are indeed MSPs, some of them may be low-mass binaries in a quiescent state. We expect them to be associated with abnormally bright stars with short orbital period. By searching the orbital periods of the optical companion stars, we may be able to obtain the spin periods of the radio-quiet MSPs from the γ-ray data.

4 CONCLUSION

We have studied the population of the γ-ray emitting MSPs using Monte Carlo techniques. We have applied the outer gap model with a switching of the gap closure process from the photon–photon pair-creation model to the magnetic pair-creation model, as suggested by Takata et al. (2010a). Using the sensitivity of the *Fermi* 6-month long observations, 9–13 radio-selected γ-ray MSPs are detected within the simulation, which is consistent with the present nine *Fermi* MSPs. The simulated distributions for the various characteristic of the radio-selected γ-ray pulsars are consistent with the present *Fermi* observations (Fig. 4). Scaling the observed sensitivity $\propto \sqrt{T}$, the present model predicts that *Fermi* should detect 15–22 radio-selected γ-ray MSPs and 95–152 γ-ray-selected MSPs over its 5-yr mission (Table 1).

Our simulation predicts that about 100 (or 200–300) γ-ray MSPs irradiate the Earth with a flux $F \geq 10^{-11}\,\mathrm{erg\,cm^{-2}\,s^{-1}}$ (or $5 \times 10^{-12}\,\mathrm{erg\,cm^{-2}\,s^{-1}}$), and most of them are categorized as γ-ray-selected pulsars with the present sensitivity of radio surveys (Fig. 5). Our simulation also predicts that about 50 per cent of the γ-ray emitting MSPs will be detected with a rotation period in the range of $P \sim 3$–$8\,\mathrm{ms}$ and a period time derivative in the range of $\dot{P} \sim 6 \times 10^{-21}$–$10^{-19}$. We further argue that γ-ray emitting MSPs are plausible as candidates for the Galactic *Fermi* unidentified steady sources, located in high Galactic latitudes. Our simulation implies that some of the radio-quiet γ-ray MSPs can be changed to radio-loud γ-ray MSPs as the simulated sensitivity of radio surveys increases. Therefore, we predict that more and more radio MSPs will be discovered in the *Fermi* unidentified sources as the radio sensitivity is improved.

REFERENCES

Abdo A. A. et al., 2009a, Sci, 325, 840
Abdo A. A. et al., 2009b, Sci, 325, 848
Abdo A. A. et al., 2009c, ApJ, 706, 1331
Abdo A. A. et al., 2010a, ApJS, 187, 460
Abdo A. A. et al., 2010b, ApJS, 188, 405
Abdo A. A. et al., 2010c, ApJ, 712, 957
Abdo A. A. et al., 2010d, ApJ, 715, 429
Aliu E. et al., 2008, Sci, 322, 1221
Archibald A. M. et al., 2009, Sci, 324, 1411
Arons J., 1983, ApJ, 266, 215
Arons J., 1993, ApJ, 408, 160
Bailes M., Kniffen D. A., 1992, ApJ, 391, 659
Binney J. J., Tremaine S. D., 1987, Galactic Dynamics. Princeton Univ. Press, Princeton, NJ
Burton W. B., Gordon M. A., 1978, A&A, 63, 7
Campana S., Colpi M., Mereghetti S., Stella L., Tavani M., 1998, A&AR, 8, 279
Caraveo P. A., 2010, in High Time REsolution Astrophysics IV – The Era of Extremely Large Telescopes – HTRA IV, Creece Ma7 5
Cheng K. S., Zhang L., 1998, ApJ, 498, 327
Cheng K. S., Ho C., Ruderman M., 1986a, ApJ, 300, 500
Cheng K. S., Ho C., Ruderman M., 1986b, ApJ, 300, 522
Cheng K. S., Ruderman M., Zhang L., 2000, ApJ, 537, 964
Cordes J. M., Lazio T. J. W., 2002, preprint (astro-ph/0207156)
Daugherty J. K., Harding A. K., 1982, ApJ, 252, 337
Daugherty J. K., Harding A. K., 1996, ApJ, 458, 278
Faucher-Giguère C.-A., Loeb A., 2010, J. Cosmol. Astropart. Phys., 1, 5
Ferrario L., Wickramasinghe D., 2007, MNRAS, 375, 1009
Frank J., King A., Raine D., 2002, Accretion Power in Astrophysics, 3rd edn. Cambridge Univ. Press, Cambridge
Goldreich P., Julian W. H., 1969, ApJ, 157, 869
Grenier I. A., 2004, preprint (astro-ph/0409096)
Harding A. K., Stern J. V., Dyks J., Frackowiak M., 2008, ApJ, 680, 1378
Hirotani K., 2008, ApJ, 688, L25
Hobbs G., Lorimer D. R., Lyne A. G., Kramer M., 2005, MNRAS, 360, 974
Jeffrey L. C., 1986, Nat, 319, 384
Kaaret P., Cottam J., 1996, ApJ, 462, L35
Kramer M., Xilouris K. M., 2000, in Kramer M., Wex N., Wielebinski R., eds, IAU Colloq. 177, Pulsar Astronomy: 2000 and Beyond. Astron. Soc. Pac., (San Francisco, p. 229
Kramer M. et al., 1997, A&A, 322, 846
Lorimer D. R., 2008 Living Rev. Relativ., 11, 8
Lorimer D. R. et al., 1995, ApJ, 439, 933
Lyne A. G., Graham-Smith F. (eds), 2006, Pulsar Astronomy, 3rd edn. Cambridge Univ. Press, Cambridge, p. 264
Manchester R. N., 1999, in Arzoumanian Z., Van der Hooft F., van den Heuvel E. P. J., eds, Pulsar Timing, General Relativity and the Internal Structure of Neutron Stars. Koninklijke Nederlandse Akademie van Wetenschappen, Amsterdam, the Netherlands, p. 53
Manchester R. N., Hobbs G. B., Teoh A., Hobbs M., 2005, AJ, 129, 1993
Muslimov A., Harding A. K., 2003, ApJ, 588, 430
Narayan R., Ostriker J. P., 1990, ApJ, 352, 222
Paczynski B., 1990, ApJ, 348, 485
Ransom S. M. et al., 2011, ApJ, 727, L16
Ray P. S., 2010, in ICREA Workshop on the High-Energy Emission from Pulsars and their Systems
Romani R. W., Watters K. P., 2010, ApJ, 714, 810
Ruderman M., 1991, ApJ, 366, 261
Ruderman M. A., Sutherland P. G., 1975, ApJ, 196, 51
Saz Parkinson P. M. et al., 2010, ApJ, 725, 571

Shklovskii I. S., 1970, SA, 13, 562
Spitkovsky A., 2006, ApJ, 648, L51
Story S. A., Gonthier P. L., Harding A. K., 2007, ApJ, 671, 713
Takata J., Chang H.-K., Shibata S., 2008, MNRAS, 386, 748
Takata J., Wang Y., Cheng K. S., 2010a, ApJ, 715, 1318
Takata J., Cheng K. S., Taam R. E., 2010b, ApJ, 723, L68
Takata J., Wang Y., Cheng K. S., 2011, ApJ, 726, 44
Venter C., Harding A. K., Guillemot L., 2009, ApJ, 707, 800

Wang Y., Takata J., Cheng K. S., 2010, ApJ, 720, 178
Watters K. P., Romani R. W., 2011, 727, 123
Zhang L., Cheng K. S., 1997, ApJ, 487, 370
Zhang L., Cheng K. S., 2003, A&A, 398, 639

This paper has been typeset from a TEX/LATEX file prepared by the author.